

E9 Berry phase effects in magnetism

Patrick Bruno

Max-Planck-Institut für Mikrostrukturphysik

Weinberg 2, D-06120 Halle, Germany

Lecture notes published in “*Magnetism goes nano*”, Lecture Manuscripts of the 36th Spring School of the Institute of Solid State Research, edited by Stefan Blügel, Thomas Brückel, and Claus M. Schneider (Forschungszentrum Jülich, 2005).

Contents

1	Introduction	3
2	Parallel transport in geometry	3
3	Parallel transport in classical mechanics: Foucault’s pendulum and the gyroscope	7
4	Parallel transport in quantum mechanics: the Berry phase	8
5	Examples of Berry phase	12
5.1	Spin in a magnetic field	12
5.2	Aharonov-Bohm effect	13
6	Experimental observations of the Berry phase for a single spin	14
6.1	Berry phase of neutrons	15
6.2	Berry phase of photons	16

6.3	Berry phase effects in nuclear magnetic resonance	17
7	Berry phase for itinerant electrons in a solid	19
7.1	General formulation	19
7.2	Anomalous Hall effect due to the Berry phase in a textured ferromagnet	20
7.3	Interference effects due to the Berry phase in an Aharonov-Bohm ring	25
8	Further effects of Berry phase in magnetism	26

1 Introduction

In 1983, Berry made the surprising discovery that a quantum system adiabatically transported round a closed circuit \mathcal{C} in the space of external parameters acquires, besides the familiar dynamical phase, a non-integrable phase depending only on the geometry of the circuit \mathcal{C} [1]. This Berry phase, which had been overlooked for more than half a century, provides us a very deep insight on the geometric structure of quantum mechanics and gives rise to various observable effects. The concept of the Berry has now become a central unifying concept in quantum mechanics, with applications in fields ranging from chemistry to condensed matter physics [2, 3].

The aim of the present lecture is to give an elementary introduction to the Berry phase, and to discuss its various implications in the field of magnetism, where it plays an increasingly important role. The reader is referred to specialized textbooks [2, 3] for a more comprehensive presentation of this topic.

2 Parallel transport in geometry

The importance of the Berry phase stems from the fact that it reveals the intimate geometrical structure underlying quantum mechanics. It is therefore appropriate to start with an introduction of the fundamental concept of *parallel transport* in a purely geometrical context; we follow here the discussion given by Berry in Ref. [4].

This is best illustrated by means of a simple example. Consider a surface Σ (e.g., a plane, a sphere, a cone, etc.) and a vector constrained to lie everywhere in the plane tangent to the surface. Next, we wish to transport the vector on the surface, *without rotating it around the axis normal to the surface*, as illustrated in Fig. 1. We are interested, in particular in the case, in which the arrow is transported round a closed circuit $\mathcal{C} \equiv (1 \rightarrow 2 \rightarrow 3 \rightarrow 1)$. We may encounter two different situations: (i) if the surface is flat, as on Fig. 1(a), then the arrow always remains parallel to its original orientation, and therefore is unchanged after completion of the circuit \mathcal{C} ; (ii) if, however, the surface Σ is curved as on Fig. 1(b,c), the arrow, being constrained to lie in the local tangent plane, cannot remain parallel to its original orientation, and after completion of the circuit \mathcal{C} , it is clearly seen to have been rotated by an angle $\theta(\mathcal{C})$, a phenomenon referred to as *anholonomy*.

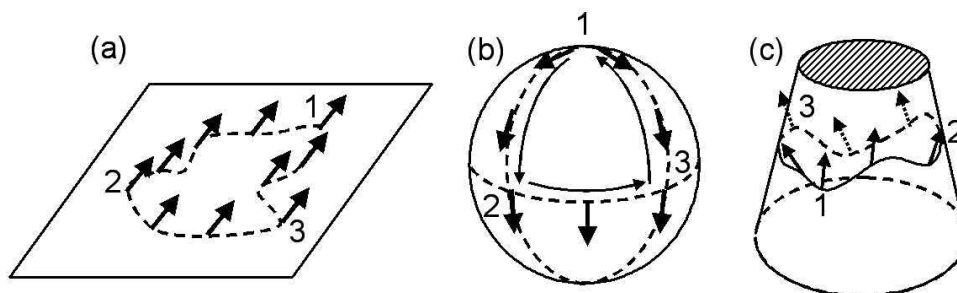


Fig. 1: Sketch of parallel transport on (a) a plane, (b) a sphere, and (c) a cone.

Let us now formalize this procedure. The arrow is represented by a tangent unit vector \mathbf{e}^1 ,

transported along a circuit $\mathcal{C} \equiv \{\mathbf{r}(t)|t = 0 \rightarrow T\}$ on the surface. Defining $\mathbf{n}(\mathbf{r})$ as the unit vector normal to the surface at point \mathbf{r} , we define a second tangent unit vector $\mathbf{e}^2 \equiv \mathbf{n} \times \mathbf{e}^1$, which is also parallel transported on the surface along \mathcal{C} . The 3 unit vectors $(\mathbf{n}, \mathbf{e}^1, \mathbf{e}^2)$ form an orthonormal reference frame. As \mathbf{e}^1 and \mathbf{e}^2 are transported, they have to rotate with an angular velocity $\boldsymbol{\omega}$ (to be determined) if the surface is not flat, i.e., the equation of motion of \mathbf{e}^1 and \mathbf{e}^2 is

$$\dot{\mathbf{e}}^r = \boldsymbol{\omega} \times \mathbf{e}^r \quad (r = 1, 2), \quad (1)$$

where the overdot indicates the time derivative. One can easily see that in order to fulfill the requirements that \mathbf{e}^1 and \mathbf{e}^2 remain tangent unit vectors (i.e., $\mathbf{e}^r \cdot \mathbf{n} = 0$, $(r = 1, 2)$) and never rotate around \mathbf{n} (i.e., $\boldsymbol{\omega} \cdot \mathbf{n} = 0$), the angular velocity has to be given by

$$\boldsymbol{\omega} = \mathbf{n} \times \dot{\mathbf{n}}. \quad (2)$$

The law of parallel transport is therefore

$$\dot{\mathbf{e}}^r = (\mathbf{n} \times \dot{\mathbf{n}}) \times \mathbf{e}^r = -(\mathbf{e}^r \cdot \dot{\mathbf{n}})\mathbf{n}. \quad (3)$$

This law can be expressed in a form more suitable for generalization to the case of quantum mechanics, by defining the complex unit vector

$$\boldsymbol{\phi} \equiv \frac{\mathbf{e}^1 + i\mathbf{e}^2}{\sqrt{2}}, \quad (4)$$

with

$$\boldsymbol{\phi}^* \cdot \boldsymbol{\phi} = 1. \quad (5)$$

The law of parallel transport now reads

$$\boldsymbol{\phi}^* \cdot \dot{\boldsymbol{\phi}} = 0. \quad (6)$$

In order to express the rotation of the unit vectors $(\mathbf{e}^1, \mathbf{e}^2)$ as they move around \mathcal{C} , we need to chose a *fixed* local orthonormal frame $(\mathbf{n}(\mathbf{r}), \mathbf{t}^1(\mathbf{r}), \mathbf{t}^2(\mathbf{r}))$ on the surface. The normal unit vector $\mathbf{n}(\mathbf{r})$ is of course uniquely determined by the surface, but we have an infinity of possible choices for $\mathbf{t}^1(\mathbf{r})$ (we simply impose that it is a smooth function of \mathbf{r}), which corresponds to a gauge freedom; once we have made a choice for $\mathbf{t}^1(\mathbf{r})$, then $\mathbf{t}^2(\mathbf{r})$ is of course uniquely determined. We next define the complex unit vector

$$\mathbf{u}(\mathbf{r}) \equiv \frac{\mathbf{t}^1(\mathbf{r}) + i\mathbf{t}^2(\mathbf{r})}{\sqrt{2}}, \quad (7)$$

with, of course,

$$\mathbf{u}^*(\mathbf{r}) \cdot \mathbf{u}(\mathbf{r}) = 1. \quad (8)$$

The relation between the parallel transported frame and the fixed one is expressed as

$$\boldsymbol{\phi}(t) = \exp[-i\theta(t)] \mathbf{u}(\mathbf{r}(t)), \quad (9)$$

where $\theta(t)$ is the angle by which $(\mathbf{t}^1, \mathbf{t}^2)$ must be rotated to coincide with $(\mathbf{e}^1, \mathbf{e}^2)$. We obtain the equation satisfied by $\theta(t)$ by inserting the above definition in the equation of parallel transport (6), and obtain

$$0 = \boldsymbol{\phi}^* \cdot \dot{\boldsymbol{\phi}} = -i \dot{\theta} \mathbf{u}^* \cdot \mathbf{u} + \mathbf{u}^* \cdot \dot{\mathbf{u}}. \quad (10)$$

Since $\mathbf{u}^* \cdot \mathbf{u} = 1$ and then $\mathbf{u}^* \cdot \dot{\mathbf{u}}$ is imaginary, we get

$$\dot{\theta} = \text{Im}(\mathbf{u}^* \cdot \dot{\mathbf{u}}), \quad (11)$$

so that

$$\theta(\mathcal{C}) = \text{Im} \oint_{\mathcal{C}} \mathbf{u}^* \cdot d\mathbf{u} \quad (12)$$

$$= - \oint_{\mathcal{C}} \mathbf{t}^2 \cdot d\mathbf{t}^1. \quad (13)$$

If we choose a coordinate system (X_1, X_2) on our surface Σ , and define the vector field $\mathbf{A}(\mathbf{r})$ (usually called a *connection*) on Σ as

$$A_i(\mathbf{X}) \equiv \text{Im} \left[u_j^*(\mathbf{X}) \frac{\partial u_j(\mathbf{X})}{\partial X_i} \right], \quad (14)$$

where we have used Einstein's convention of summation over repeated indices, we get

$$\theta(\mathcal{C}) = \oint_{\mathcal{C}} \mathbf{A}(\mathbf{X}) \cdot d\mathbf{X}, \quad (15)$$

which constitutes the *1-form* expression of the anholonomy angle $\theta(\mathcal{C})$. The connection $\mathbf{A}(\mathbf{X})$ depends on our particular gauge choice for $\mathbf{t}^1(\mathbf{X})$: if we make a new choice $\mathbf{t}'^1(\mathbf{X})$ which is brought in coincidence with $\mathbf{t}^1(\mathbf{X})$ by a rotation of angle $\mu(\mathbf{X})$, i.e., if we make the gauge transformation

$$\mathbf{u}(\mathbf{X}) \rightarrow \mathbf{u}'(\mathbf{X}) \equiv \exp(-i\mu(\mathbf{X})) \mathbf{u}(\mathbf{X}), \quad (16)$$

we obtain a new connection

$$A'_i(\mathbf{X}) \equiv \text{Im} \left[u_j'^*(\mathbf{X}) \frac{\partial u_j'(\mathbf{X})}{\partial X_i} \right] = A_i(\mathbf{X}) - \frac{\partial \mu(\mathbf{X})}{\partial X_i}. \quad (17)$$

However, since

$$\oint_{\mathcal{C}} \nabla \mu(\mathbf{r}) \cdot d\mathbf{r} = \oint_{\mathcal{C}} d\mu(\mathbf{r}) = 0, \quad (18)$$

we can see that the expression (15) for the anholonomy angle $\theta(\mathcal{C})$ is indeed gauge invariant, as it should.

A more intuitive understanding of the anholonomy angle may be obtained if we use Stokes' theorem to express it as a surface integral. In doing so, however, we should pay attention to the possible existence of holes in the surface Σ . If this is the case, Σ is said to be non simply connected. An example is sketched on Fig. 2, where the surface Σ has 2 holes limited by the contours \mathcal{C}_1 and \mathcal{C}_2 (hatched areas on Fig. 2). Applying Stokes theorem, we then obtain

$$\theta(\mathcal{C}) = \iint_{\mathcal{S}} B(\mathbf{X}) dX_1 dX_2 + \sum_i N_i(\mathcal{C}) \theta(\mathcal{C}_i). \quad (19)$$

where the surface \mathcal{S} is the subset of the surface Σ limited by the circuit (dotted area on Fig. 2), \mathcal{C} , $N_i(\mathcal{C})$ is the winding number of circuit \mathcal{C} around the hole i (i.e., the difference between the number of turns in counterclockwise and clockwise directions),

$$\theta(\mathcal{C}_i) \equiv \oint_{\mathcal{C}_i} \mathbf{A}(\mathbf{X}) \cdot d\mathbf{X} \quad (20)$$

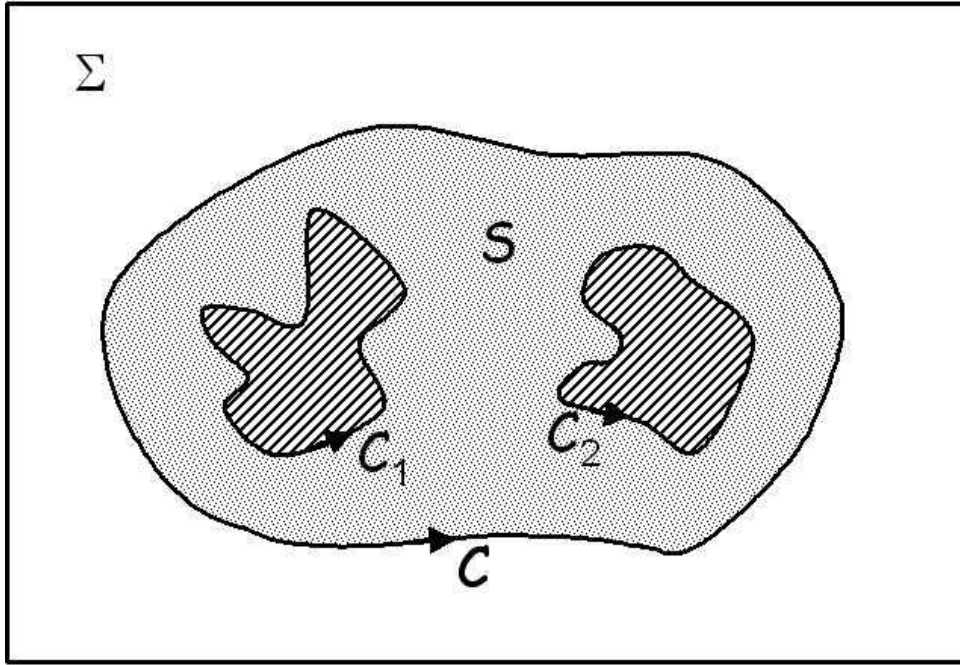


Fig. 2: Sketch of a non simply connected surface Σ , with 2 holes (hatched areas), limited by the contours C_1 and C_2 .

is the anholonomy angle of circuit C_i and

$$\begin{aligned} B(\mathbf{X}) &\equiv \left(\frac{\partial A_2}{\partial X_1} - \frac{\partial A_1}{\partial X_2} \right) \\ &= \text{Im} \left[\frac{\partial \mathbf{u}^*}{\partial X_1} \cdot \frac{\partial \mathbf{u}}{\partial X_2} - \frac{\partial \mathbf{u}^*}{\partial X_2} \cdot \frac{\partial \mathbf{u}}{\partial X_1} \right]. \end{aligned} \quad (21)$$

Equation (19) constitutes the 2-form expression of the anholonomy angle $\theta(C)$. One can see immediately that, unlike the connection $\mathbf{A}(\mathbf{X})$, the quantity $B(\mathbf{X})$ is gauge invariant. The geometrical meaning of $B(\mathbf{X})$ stems from its relation to the *Gaussian curvature* K of Σ at point \mathbf{X} , i.e.,

$$B(\mathbf{X})dX_1dX_2 = KdS \equiv \frac{dS}{R_1(\mathbf{X})R_2(\mathbf{X})}, \quad (22)$$

where $R_1(\mathbf{X})$ and $R_2(\mathbf{X})$ are the principal curvature radii at point \mathbf{X} . In the case of the sphere, this is easily checked by explicit calculation, taking the usual spherical angles (θ, φ) as variables (X_1, X_2) . Since the Gaussian curvature is related to the solid angle Ω of spanned by the normal unit vector \mathbf{n} by

$$B = \frac{d^2\Omega}{dX_1dX_2} \quad (23)$$

we finally get

$$\theta(C) - \sum_i N_i(C)\theta(C_i) = \iint_S \frac{d^2\Omega}{dX_1dX_2} dX_1dX_2 = \iint_S d^2\Omega = \Omega(S), \quad (24)$$

where $\Omega(S)$ is the solid angle described by the normal vector \mathbf{n} on the surface S . That the above results hold not only for a sphere, but for any surface can be understood easily from the

following argument: Eq. (3) shows that the trajectory of the parallel transported tangent vectors is entirely determined by the trajectory of the normal unit vector \mathbf{n} along \mathcal{C} . We can therefore map the trajectory \mathcal{C} on the surface Σ to a trajectory \mathcal{C}' on the sphere of unit radius S^2 , by mapping each point of Σ onto the point of S^2 with the same normal vector \mathbf{n} . This implies that we can restrict ourselves to studying the case of parallel transport on S^2 and obtain conclusions valid for parallel transport on any surface Σ .

Let us examine these results for the examples sketched on Fig. 1. For the case of the plane, the anholonomy of course trivially vanishes. For the sphere, the anholonomy angle is given by the solid angle $\Omega(\mathcal{S})$, and is therefore a *geometric* property of the circuit \mathcal{C} ; this can be easily checked by making the following experiment: take your pen in your left hand, and raise your arm above your head, the pen pointing in front of you; then rotate your arm until it is horizontal in front of you, without twisting your hand; then rotate it by 90° to your left; finally rotate your arm back to the vertical (pay attention to never twist your hand in whole process); the pen is now pointing to your left, i.e., it has rotated by $4\pi/8 = \pi/2$. For the case of the cone, the Gaussian curvature vanishes everywhere (a cone can be fabricated by rolling a sheet of paper), so that the anholonomy angle is in fact a *topological* property of the circuit \mathcal{C} , being given by the winding number of the circuit \mathcal{C} around the cone (multiplied by the solid angle of the cone).

3 Parallel transport in classical mechanics: Foucault's pendulum and the gyroscope

Let us now consider the famous experiment of Foucault's pendulum that demonstrated the earth's rotation. If the pendulum trajectory is originally planar (swinging oscillation), the vertical component of the angular momentum vanishes. Since forces exerted on the pendulum (gravity and wire tension) produce a vanishing vertical torque, the vertical component of the angular momentum has to be conserved. The absence of any vertical torque imposes that the swing plane has to follow a law of parallel transport as the direction of gravity slowly changes due to the earth's rotation. Therefore, within one day it rotates by an angle equal to the solid angle described by the vertical $2\pi(1 - \cos \theta)$, where θ is the colatitude.

The parallel transport may also affect the phase of the periodic motion of the Foucault pendulum or the rotation phase of a gyroscope, but also the phase of their periodic motion. Let us consider a gyroscope whose rotation axis is constrained to remain parallel to the axis \mathbf{n} ; let us now move the rotation axis \mathbf{n} round a closed circuit \mathcal{C} . The rotation angle of the gyroscope will be the sum of the *dynamic rotation angle* ωt and of a *geometric anholonomy angle* $\theta(\mathcal{C})$ equal to the solid angle described by the rotation axis. Thus if we have two synchronous gyroscopes and perform different circuits with the rotation axes, they will eventually be dephased with respect to each other, an effect that could easily be observed by stroboscopy. This geometric anholonomy angle is known as Hannay's angle [5, 6]. If the Foucault pendulum is given a conical oscillation, instead of a planar swing, then we have exactly the same situation as described above for the gyroscope, and the rotation angle will have an anholonomy excess angle given by the solid angle described by the vertical. Thus, two identical Foucault pendula (i.e., of same length) with circular oscillations in opposite directions will have slightly different oscillation frequencies, and will progressively get dephased with respect to each other. The swinging motion of the

usual Foucault may be view as the superposition of circular motions in opposite direction, so that the rotation of the swinging plane may be viewed as resulting from the above mentioned frequency shift.

4 Parallel transport in quantum mechanics: the Berry phase

Let us now consider a quantum mechanical system described by a Hamiltonian controlled by a set of external parameters (R_1, R_2, \dots) , which we describe collectively as a vector \mathbf{R} in some abstract parameter space. Physically, the external parameters may be magnetic or electric fields, etc. For each value \mathbf{R} of the external parameters, the Hamiltonian $H(\mathbf{R})$ has eigenvalues $E_n(\mathbf{R})$ and eigenvectors $|n(\mathbf{R})\rangle$ satisfying the independent Schrödinger equation, i.e.,

$$H(\mathbf{R}) |n(\mathbf{R})\rangle = E_n(\mathbf{R}) |n(\mathbf{R})\rangle \quad (25)$$

The eigenvectors $|n(\mathbf{R})\rangle$ are defined up to an arbitrary phase, and there is *a priori* no particular phase relation between eigenstates corresponding to different values of the parameter \mathbf{R} . We make a particular choice for the phase of the eigenstates, simply requiring that $|n(\mathbf{R})\rangle$ varies smoothly with \mathbf{R} in the region of interest. It may happen that the eigenstates we have chosen are not single valued functions of \mathbf{R} . If this happens, special care must be given to this point.

Let us perform an adiabatic closed circuit $\mathcal{C} \equiv \{\mathbf{R}(t)|t = 0 \rightarrow T\}$ in the parameter space. The adiabatic theorem [7] tells us that if the rate of variation of the external parameters is low enough, a system that is initially in the n th stationary state $|n\rangle$ (assumed non-degenerate) of the Hamiltonian will remain continuously in the state $|n\rangle$. The condition of adiabaticity is that the stationary state under consideration remains non-degenerate, and the rate of variation of the Hamiltonian is low enough to make the probability of transition to another state $|m\rangle$ vanishingly small, i.e.,

$$\hbar |\langle m | \dot{H} | n \rangle| \ll |E_m - E_n|^2 \quad \forall m \neq n. \quad (26)$$

Then of course, if one performs a closed adiabatic circuit \mathcal{C} , the system has to return to its original state.

Berry [1] asked the following question: what will be the phase of the state after completion of the circuit \mathcal{C} ? It may be difficult at first sight to realize that this question may be of any interest. Indeed, the expectation value of any observable quantity A ,

$$\langle A \rangle \equiv \langle \psi | A | \psi \rangle \quad (27)$$

does not depend of the phase of $|\psi\rangle$. This lack of interest is certainly the main reason why the Berry phase was (almost ¹) completely overlooked for more than half a century of quantum mechanics.

So, following Berry, taking

$$|\psi(t = 0)\rangle \equiv |n(\mathbf{R}(t = 0))\rangle \quad (28)$$

¹Some early precursor work on effects related to the Berry phase include notably Pancharatnam's work on optical polarization [8], Aharonov and Bohm's work on the phase due to the electromagnetic potential vector [9], and Mead and Truhlar's work on the molecular Aharonov-Bohm effect in the Born-Oppenheimer theory of molecular vibrations [10].

we express the state $|\psi(t)\rangle$ at a latter time t as

$$|\psi(t)\rangle \equiv \exp\left[\frac{-i}{\hbar} \int_0^t dt' E_n(\mathbf{r}(t'))\right] |\phi_n(t)\rangle, \quad (29)$$

i.e., we introduce an auxiliary wavefunction $|\phi_n(t)\rangle$ with a zero dynamical phase. Using the time-dependent Schrödinger equation,

$$i\hbar|\dot{\psi}(t)\rangle = H(t)|\psi(t)\rangle, \quad (30)$$

and projecting it on $\langle\psi(t)|$, we get

$$\begin{aligned} 0 &= \langle\psi(t)| \left(H(t) - i\hbar \frac{\partial}{\partial t} \right) |\psi(t)\rangle \\ &= \langle\phi_n(t)| \dot{\phi}_n(t)\rangle, \end{aligned} \quad (31)$$

where we have used the relation

$$\langle\psi(t)| H(t) |\psi(t)\rangle = E_n(t), \quad (32)$$

which follows from the adiabatic theorem. Equation (31) shows that the wavefunction $|\phi_n(t)\rangle$ obeys a quantum mechanical analogue of the law of parallel transport (6).

In complete analogy with the problem of parallel transport on a surface, we now express the parallel transported state $|\phi_n(t)\rangle$ in terms of the fixed eigenstates $|n(\mathbf{R})\rangle$ as

$$|\phi_n(t)\rangle \equiv \exp(i\gamma_n(t)) |n(\mathbf{R})\rangle, \quad (33)$$

where the phase $\gamma_n(t)$ plays the same role as the angle $-\theta(t)$ for the problem of parallel transport on a surface. We then immediately get the equation of motion of $\gamma_n(t)$, i.e.,

$$\dot{\gamma}_n(t) = i\langle n|\dot{n}\rangle = -\text{Im}\langle n(\mathbf{R}(t))|\frac{d}{dt}n(\mathbf{R}(t))\rangle, \quad (34)$$

which is analogous to Eq. (11).

Finally, the answer to the question originally asked by Berry is

$$|\psi(T)\rangle = \exp[i(\delta_n + \gamma_n(\mathcal{C}))] |\psi(0)\rangle, \quad (35)$$

where

$$\delta_n \equiv \frac{-1}{\hbar} \int_0^T E_n(\mathbf{R}(t)) dt \quad (36)$$

is the dynamical phase, and

$$\gamma_n(\mathcal{C}) \equiv -\text{Im} \left[\oint_{\mathcal{C}} \langle n(\mathbf{R})|\partial_{\mathbf{R}}|n(\mathbf{R})\rangle \cdot d\mathbf{R} \right] - \alpha_n(\mathcal{C}) \quad (37)$$

is the Berry phase. The last term in the latter equation arises when the states $|n(\mathbf{R})\rangle$ are not a single-valued function of \mathbf{R} in the region of interest of the parameter space², and is given by

$$\alpha_n(\mathcal{C}) = i \ln [\langle n(\mathbf{R}(0))|n(\mathbf{R}(T))\rangle]. \quad (38)$$

²This term was absent in Berry's original paper [1], because the basis states $|n(\mathbf{R})\rangle$ were assumed to be single-valued.

We shall omit this term below, and consider only the case of single-valued basis states.

We note the very close analogy between the result obtained for quantum and classical systems. The dynamical phase of a quantum system is analogous to the rotation angle ωT in classical mechanics, whereas the Berry phase is analogous to Hannay's angle (they both arise from the anholonomy of parallel transport).

Defining the connection $\mathbf{A}^n(\mathbf{R})$ as

$$\mathbf{A}^n(\mathbf{R}) \equiv -\text{Im} [\langle n(\mathbf{R}) | \partial_{\mathbf{R}} n(\mathbf{R}) \rangle], \quad (39)$$

we re-express the Berry phase as

$$\gamma_n(\mathcal{C}) \equiv \oint_{\mathcal{C}} \mathbf{A}^n(\mathbf{R}) \cdot d\mathbf{R}, \quad (40)$$

which constitutes the 1-form expression of the Berry phase. The latter clearly depends only on the geometry of the circuit \mathcal{C} . The connection $\mathbf{A}^n(\mathbf{R})$ is not gauge invariant: if we make a new choice for the phase of the reference state, i.e.,

$$|n(\mathbf{R})\rangle' = \exp(-i\mu(\mathbf{R}))|n(\mathbf{R})\rangle, \quad (41)$$

with a single-valued function $\mu(\mathbf{R})$, we obtain a different connection

$$\mathbf{A}^{n'}(\mathbf{R}) = \mathbf{A}^n(\mathbf{R}) + \partial_{\mathbf{R}}\mu(\mathbf{R}). \quad (42)$$

However, the Berry phase $\gamma_n(\mathcal{C})$ is gauge invariant, as it should.

As for the geometric parallel transport on surfaces, we may obtain a gauge invariant and more transparent expression by transforming the above result to a surface integral by using Stokes' theorem. Here too, we have to pay attention to the existence of holes in the parameter space: if the parameter space is multiply connected, and if the circuit \mathcal{C} cannot be continuously deformed to a point³, we must take into account terms associated with the winding of \mathcal{C} around holes of the parameter space.

The formulation of the Berry phase as a surface integral in a form that is independent of a particular choice of coordinates of the parameter space generally requires to use the mathematical formalism of differential forms [3], which is beyond the scope of the present lecture. We can nevertheless obtain a useful result without resorting to any advanced mathematics if we make a suitable choice of coordinates of the parameter space. Let us choose a surface \mathcal{S} in the parameter space which is bound by the circuit \mathcal{C} , and a parameterization (R_1, R_2) of the surface \mathcal{S} . Using Stokes' theorem we then get

$$\gamma_n(\mathcal{C}) = \iint_{\mathcal{S}} B^n(\mathbf{R}) dR_1 dR_2 + \sum_i N_i(\mathcal{C}) \gamma_n(\mathcal{C}_i), \quad (43)$$

where \mathcal{C}_i are the circuits bounding the holes of the parameter space and N_i the corresponding winding numbers of the circuit \mathcal{C} around them, and where

$$\begin{aligned} B^n(\mathbf{R}) &\equiv (\partial_{R_1} A_2^n - \partial_{R_2} A_1^n) \\ &= -\text{Im} [\langle \partial_{R_1} n(\mathbf{R}) | \partial_{R_2} n(\mathbf{R}) \rangle - \langle \partial_{R_2} n(\mathbf{R}) | \partial_{R_1} n(\mathbf{R}) \rangle] \end{aligned} \quad (44)$$

³A circuit that can be continuously deformed to a point is said to be *homotopic* to a point.

is the *Berry curvature*. In the case where the parameter space is three-dimensional, then we can use the familiar language of vector calculus, as in electrodynamics, and Stokes' theorem yields

$$\gamma_n(\mathcal{C}) = \iint_S \mathbf{B}^n(\mathbf{R}) \cdot \mathbf{n} \, dS + \sum_i N_i(\mathcal{C}) \gamma_n(\mathcal{C}_i), \quad (45)$$

$$\begin{aligned} \mathbf{B}^n(\mathbf{R}) &\equiv \nabla \times \mathbf{A}^n(\mathbf{R}) \\ &= -\text{Im} [\langle \nabla n(\mathbf{R}) | \times | \nabla n(\mathbf{R}) \rangle] \end{aligned} \quad (46)$$

$$= -\text{Im} \sum_{m \neq n} \langle \nabla n(\mathbf{R}) | m(\mathbf{R}) \rangle \times \langle m(\mathbf{R}) | \nabla n(\mathbf{R}) \rangle. \quad (47)$$

Making use of the relation

$$\langle m | \nabla n \rangle = \frac{\langle m | \nabla H | n \rangle}{E_n - E_m}, \quad (48)$$

one eventually get

$$\mathbf{B}^n(\mathbf{R}) = -\text{Im} \sum_{m \neq n} \frac{\langle n(\mathbf{R}) | \nabla H(\mathbf{R}) | m(\mathbf{R}) \rangle \times \langle m(\mathbf{R}) | \nabla H(\mathbf{R}) | n(\mathbf{R}) \rangle}{(E_m(\mathbf{R}) - E_n(\mathbf{R}))^2}. \quad (49)$$

Obviously, the Berry curvature is gauge invariant. As the notation suggests, the Berry curvature \mathbf{B}^n plays the role of a magnetic field in the space of parameters, whose vector potential is the Berry connection \mathbf{A}^n .

The energy denominator in Eq. (49) shows that if the circuit \mathcal{C} lies in a region of the parameter space that is close to a point \mathbf{R}^* of two-fold degeneracy involving the two states labelled + and -, the corresponding Berry connections \mathbf{B}^+ and \mathbf{B}^- are dominated by the term involving the denominator $(E_+ - E_-)^2$ and the contribution involving other states can be neglected. So, to first order in $\mathbf{R} - \mathbf{R}^*$, one has

$$\mathbf{B}_+(\mathbf{R}) = -\mathbf{B}_-(\mathbf{R}) = -\text{Im} \frac{\langle +(\mathbf{R}) | \nabla H(\mathbf{R}^*) | -(\mathbf{R}) \rangle \times \langle -(\mathbf{R}) | \nabla H(\mathbf{R}^*) | +(\mathbf{R}) \rangle}{(E_+(\mathbf{R}) - E_-(\mathbf{R}))^2}. \quad (50)$$

The general form of the Hamiltonian $H(\mathbf{R})$ of a two-level system is (without loss of generality, we may take $\mathbf{R}^* = 0$)

$$H(\mathbf{R}) \equiv \frac{1}{2} \begin{pmatrix} Z & X - iY \\ X + iY & -Z \end{pmatrix}, \quad (51)$$

with eigenvalues

$$E_+(\mathbf{R}) = -E_-(\mathbf{R}) = \frac{1}{2}R. \quad (52)$$

This illustrates a theorem due to von Neumann and Wigner [11], stating that it is necessary to adjust 3 independent parameters in order to obtain a two-fold degeneracy from an Hermitian matrix. The gradient of the Hamiltonian is

$$\nabla H = \frac{1}{2} \boldsymbol{\sigma}, \quad (53)$$

where $\boldsymbol{\sigma}$ is the vector matrix whose components are the familiar Pauli matrices. Simple algebra then yields

$$\mathbf{B}_+ = -\mathbf{B}_- = -\frac{\mathbf{R}}{R^3}. \quad (54)$$

The above Berry curvature \mathbf{B}_\pm is the magnetic field in parameter space generated by a Dirac magnetic monopole [12] of strength $\mp 1/2$. Thus, the Berry phase $\gamma_\pm(\mathcal{C})$ of a circuit \mathcal{C} is given by the flux of the monopole through the surface \mathcal{S} subtended by the circuit \mathcal{C} , which, by Gauss' theorem, is nothing else as $\mp\Omega(\mathcal{C})$, where $\Omega(\mathcal{C})$ is the solid angle described by \mathbf{R} along the circuit \mathcal{C} .

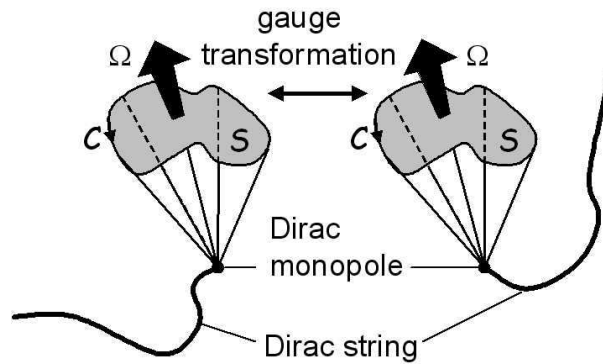


Fig. 3: Sketch showing the flux of the Dirac monopole through the circuit \mathcal{C} , and the effect of a gauge transformation.

The corresponding vector potential (or Berry connection) \mathbf{A}_\pm (not calculated here), has an essential singularity along a line (Dirac string) ending at the origin, and carrying a "flux" of magnitude $\pm 2\pi$. The position of the Dirac string can be moved (but not removed!) by a gauge transformation, as sketched on Fig. 3. If the Dirac string happens to cross the cross the surface \mathcal{S} , the Berry phase remains unchanged (modulo 2π), so that the result is indeed gauge invariant.

5 Examples of Berry phase

5.1 Spin in a magnetic field

As a first example, we consider the case of a single spin (of magnitude S) in a magnetic field, which is both the most immediate application of the formal theory presented above and one of the most frequent case encountered in experimentally relevant situations. The Hamiltonian considered is

$$H(\mathbf{b}) \equiv -\mathbf{b} \cdot \mathbf{S}, \quad (55)$$

with the magnetic field \mathbf{b} being the external parameters. The eigenvalues are

$$E_n(\mathbf{b}) = -nb, \quad (56)$$

with $2n$ integer and $-S \leq n \leq S$. For $\mathbf{b} = 0$, the $2S + 1$ eigenstates are degenerate, so the circuit \mathcal{C} has to avoid the origin. The Berry connection can be calculated using Eq. (49) and well known properties of the spin operators, and one gets

$$\mathbf{B}^n(\mathbf{b}) = -n \frac{\mathbf{b}}{b^3}, \quad (57)$$

which is the "magnetic field" (in parameter space) of a monopole of strength $-n$ located at the origin. The Berry phase is thus

$$\gamma_n(\mathcal{C}) = -n\Omega(\mathcal{C}), \quad (58)$$

where $\Omega(\mathcal{C})$ is the solid angle described by the field \mathbf{b} along the circuit \mathcal{C} . For $S = 1/2$, this of course reduces to the result obtained above for the two-level problem. Note that the Berry phase $\gamma_n(\mathcal{C})$ depends only on the quantum number n (projection of \mathbf{S} on \mathbf{b}) and not on the magnitude S of the spin. Note also, that while $H(\mathbf{b})$ is the most general Hamiltonian for a spin $S = 1/2$, this is not the case for a spin $S \geq 1$; in the latter case we are restricting ourselves here to a subspace of the full parameter space. If a more general Hamiltonian and a wider parameter space is considered, the simple result obtained above would not hold any more.

5.2 Aharonov-Bohm effect

Another example which is a great interest, both conceptually and experimentally, is the well known Aharonov-Bohm effect [9]. We follow here the presentation of the Aharonov-Bohm effect given by Berry [1].

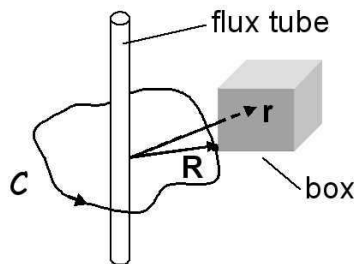


Fig. 4: Sketch describing the Aharonov-Bohm effect.

Let us consider the situation depicted in Fig. 4, namely a magnetic field confined in a tube with flux Φ and a box located at \mathbf{R} in which particles of charge q are confined. The magnetic field vanishes everywhere outside the flux tube, and in particular inside the box. Let $\mathbf{A}(\mathbf{r})$ be the corresponding vector potential. The latter generally does not vanish in the regions of vanishing field (unless the flux Φ is a multiple of the flux quantum $\Phi_0 \equiv h/e$).

Let the Hamiltonian describing the particles in the box be $H(\mathbf{p}, \mathbf{r} - \mathbf{R})$; the corresponding wave functions, for a vanishing vector potential, are of the form $\psi_n(\mathbf{r} - \mathbf{R})$, with energies E_n independent of \mathbf{R} . When the flux is non-zero, we can choose as basis states $|n(\mathbf{R})\rangle$, satisfying

$$H(\mathbf{p} - q\mathbf{A}(\mathbf{r}), \mathbf{r} - \mathbf{R})|n(\mathbf{R})\rangle = E_n|n(\mathbf{R})\rangle, \quad (59)$$

whose solutions are given by

$$\langle \mathbf{r} | n(\mathbf{R}) \rangle = \exp \left[\frac{iq}{\hbar} \int_{\mathbf{R}}^{\mathbf{r}} d\mathbf{r}' \cdot \mathbf{A}(\mathbf{r}') \right] \psi_n(\mathbf{r} - \mathbf{R}), \quad (60)$$

where the integral is performed along a path contained in the box. The energies E_n are independent of the vector potential, because it is always possible to find a gauge transformation that would make it zero in the box (but not everywhere in space!).

The Hamiltonian depends on the position \mathbf{R} of the box via the vector potential. Thus our parameter space, in this example, is nothing else than the real space, with exclusion of the region of the flux tube. If we transport the box around a closed circuit \mathcal{C} , the Berry phase will be given by

$$\gamma_n(\mathcal{C}) \equiv \oint_{\mathcal{C}} \mathbf{A}^n(\mathbf{R}) \cdot d\mathbf{R}, \quad (61)$$

with the Berry connection

$$\begin{aligned} \mathbf{A}^n(\mathbf{R}) &\equiv -\text{Im} [\langle n(\mathbf{R}) | \partial_{\mathbf{R}} n(\mathbf{R}) \rangle] \\ &= -\text{Im} \iiint d^3\mathbf{r} \psi_n^*(\mathbf{r} - \mathbf{R}) \left[\frac{-iq}{\hbar} \mathbf{A}(\mathbf{R}) \psi_n(\mathbf{r} - \mathbf{R}) + \partial_{\mathbf{R}} \psi_n(\mathbf{r} - \mathbf{R}) \right] \\ &= \frac{q}{\hbar} \mathbf{A}(\mathbf{R}). \end{aligned} \quad (62)$$

The Berry curvature $\mathbf{B}^n(\mathbf{R}) = \nabla \times \mathbf{A}^n(\mathbf{R}) = (q/\hbar)\mathbf{B}(\mathbf{R})$ is just given by the magnetic field, and vanishes everywhere outside the flux tube. But because the tube region is excluded from the allowed parameter space, the latter is multiply connected, and the Berry phase is purely topological, being given by the winding number $N(\mathcal{C})$ of the circuit \mathcal{C} around the flux tube, and by the flux Φ :

$$\gamma_n(\mathcal{C}) = 2\pi N(\mathcal{C}) \frac{q}{\hbar} \Phi. \quad (63)$$

The Aharonov-Bohm effect was confirmed experimentally by electron holography by Tonomura *et al.* [13] in a configuration where the magnetic truly vanishes, and plays an outstanding role in the physics of mesoscopic systems, where it gives rise to conductance oscillations and to persistent currents in mesoscopic metallic rings threaded by a magnetic flux [14, 15, 16].

6 Experimental observations of the Berry phase for a single spin

Let us now discuss how the Berry phase could be detected experimentally. As already mentioned, this is not immediately clear since the expectation value of any observable would be independent of the phase of the system. As always when considering phases, some kind of interference has to be observed. There various ways in which this can be done.

- Berry original proposal [1] was the following: a monoenergetic polarized beam of particles in the spin state n along the magnetic field \mathbf{b} is split in two beams. For one of the beams, the field \mathbf{b} is kept constant in magnitude and direction, whereas in the second beam, the magnitude of \mathbf{b} is kept constant and its direction slowly varied along a circuit \mathcal{C} subtending a solid angle Ω . The two beams are then recombined to interfere, and the intensity is monitored as a function of the solid angle Ω . Since the dynamical phase is the same for both beams, the phase difference between the two beams is given purely by the Berry phase (plus a propagation factor is determined by the phase shift for $\Omega = 0$). Although conceptually possible, it seems unlikely that such an experiment would be feasible in practice. In particular, it would be extremely difficult to ensure that the difference between the dynamical phases of the two beams be smaller than the Berry phase one wants

to detect, unless some physical principle enforces it. This kind of experiment may be said to be of type "one state – two Hamiltonians". This kind of experiment, being based on interferences is truly quantum mechanical.

- An alternative approach, more amenable to experimental test is to prepare the system into a superposition of two states, i.e.,

$$|\psi(t=0)\rangle = \alpha|n(\mathbf{R}(t=0))\rangle + \beta|m(\mathbf{R}(t=0))\rangle, \quad (64)$$

with $m = n - 1$ and $|\alpha|^2 + |\beta|^2 = 1$, for example by polarizing it along a direction perpendicular to the field \mathbf{b} . The orientation of the transverse component of the spin is given by the angle $\theta(t=0) \equiv \arg(\beta) - \arg(\alpha)$. The spin of course precesses at around \mathbf{b} at the Larmor frequency $\omega_L = b/\hbar$. After completion of the circuit \mathcal{C} , the system state has evolved to

$$|\psi(T)\rangle = \alpha \exp[i(\delta_n + \gamma_n(\mathcal{C}))]|n(\mathbf{R}(t=0))\rangle + \beta \exp[i(\delta_m + \gamma_m(\mathcal{C}))]|m(\mathbf{R}(t=0))\rangle, \quad (65)$$

and the polarization angle has evolved to $\theta(T) = \theta(t=0) + \Delta\theta$ with

$$\Delta\theta = \Delta\theta_{\text{dyn}} + \Delta\theta_{\text{B}}, \quad (66)$$

$$\Delta\theta_{\text{dyn}} \equiv \delta_m - \delta_n = \omega_L T, \quad (67)$$

$$\Delta\theta_{\text{B}} \equiv \gamma_m(\mathcal{C}) - \gamma_n(\mathcal{C}). \quad (68)$$

Here the angle $\Delta\theta_{\text{dyn}}$ gives the polarization rotation due to the Larmor precession (dynamic phase), while $\Delta\theta_{\text{B}}$ is the polarization rotation due to the Berry phase accumulated along the circuit \mathcal{C} . Thus by investigating how the polarization varies as the circuit \mathcal{C} is modified, the Berry phase can be detected. Such an experiment may be said to be of the type "two states – one Hamiltonian". Note that this type of experiment can be interpreted in purely classical terms [17] (it bears a clear analogy to the rotation of swinging plane of the Foucault pendulum); this is related to the fact that only Berry phase differences between two states, and not the absolute Berry phase of a given state is detected.

- A further possibility consists in repeating the circuit \mathcal{C} in a periodic manner. Thus, the Berry phase is accumulated linearly in time, just as the dynamical phase, and leads to an apparent energy shift for the state n ,

$$\Delta E_n = \frac{\hbar}{T} \gamma_n(\mathcal{C}), \quad (69)$$

which gives rise to an observable shift of the transition between to levels n and m . Such an experiment is of type "two states – one Hamiltonian", too. It can also be interpreted in classical terms and has close analogy to the period shift of a Foucault pendulum with circular oscillation.

6.1 Berry phase of neutrons

The Berry phase has been observed for neutrons by Bitter and Dubbers [18], who used the experimental shown in Fig. 5. A slow ($v \simeq 500 \text{ m.s}^{-1}$), monochromatic, beam neutrons polarized

($P \simeq 0.97$) along an axis perpendicular to the beam axis z is injected in a cylinder with a helical magnetic field with longitudinal component B_z and transverse component B_1 making a right-handed turn of 2π . Depending on the values of B_z and B_1 , various values of the solid angle Ω may be achieved.

After having traversed the cylinder, the polarization of the beam is measured, from which the Berry phase can be extracted. The comparison of the measured Berry phase (or more precisely the difference of Berry phase between states $S_z = +1/2$ and $S_z = -1/2$) and of the solid angle is shown in Fig. 5. The observation is in good agreement with the theoretical prediction.

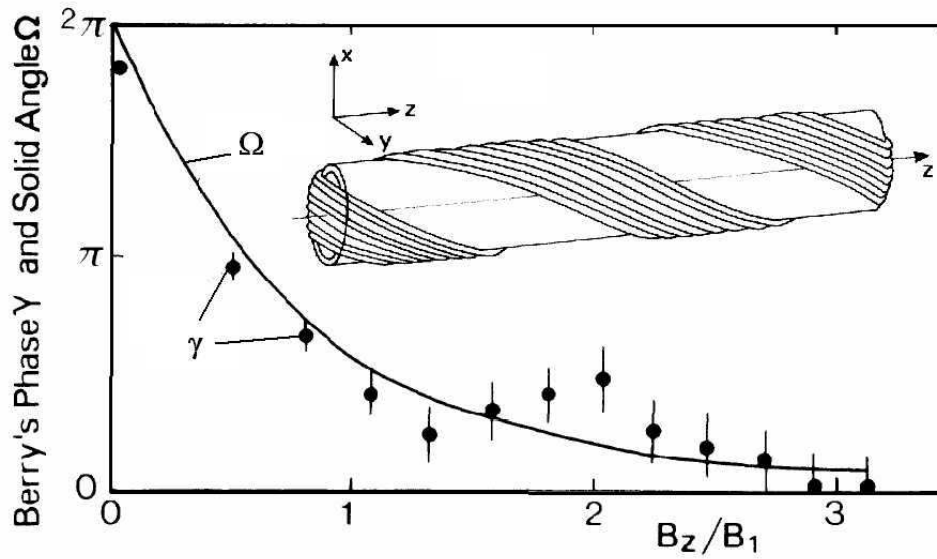


Fig. 5: Measurement of Berry phase of neutrons. The inset shows the arrangement of the coil giving an helical field; the neutron beam is along z ; length: 40 cm, diameter: 8 cm; an axial coil (not shown) produces a field B_z . The curve shows the Berry phase (more precisely $\gamma_{-1/2} - \gamma_{1/2}$) and solid angle Ω as a function of the ratio B_z/B_1 . From Ref. [18].

6.2 Berry phase of photons

The photon is a particle of spin $S = 1$ and can thus experience a Berry phase. The particularity of the photon is that, being massless, only the states $S_z = \pm 1$ occur and that the quantization axis is fixed by the direction of the wave vector \mathbf{k} . The wavevector therefore plays the role of a magnetic field for the photon [19].

If the latter is constrained to make a closed circuit \mathcal{C} of solid angle Ω , then a Berry phase of $\pm\Omega$ is expected for the two circular polarizations, respectively. If a monochromatic, linearly polarized, optical wave

$$|\chi\rangle = \frac{|+\rangle + |-\rangle}{\sqrt{2}}, \quad (70)$$

where $|+\rangle$ and $|-\rangle$ represent, respectively the two circular polarization modes, is injected in a single mode optical fiber, whose axis describes a helix of solid angle Ω , then the emerging wave

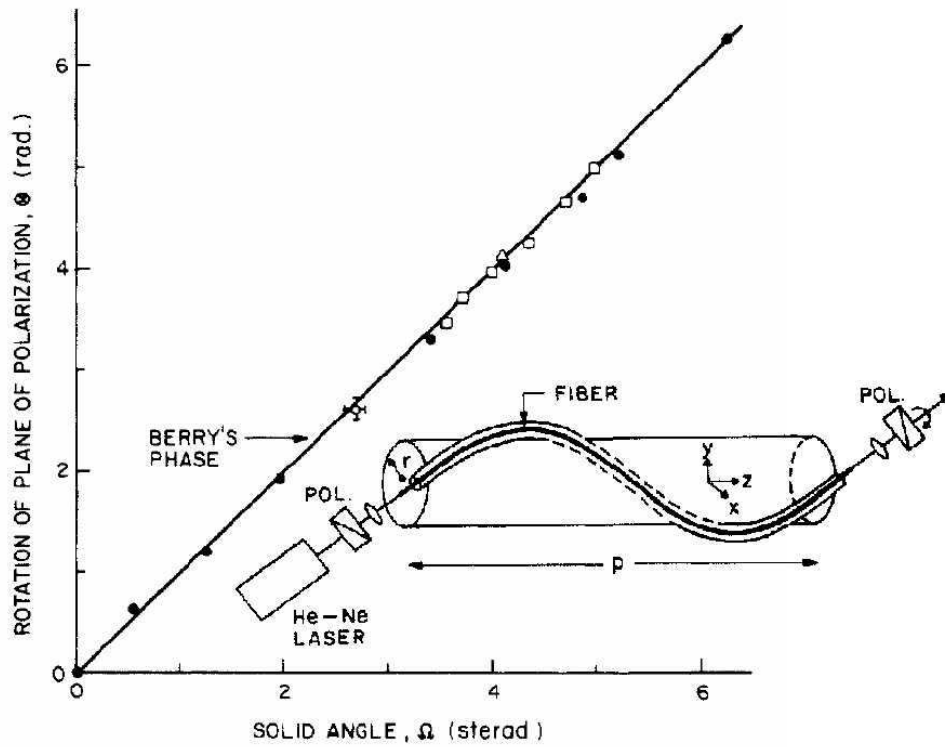


Fig. 6: Berry phase measurement for photons. The inset shows the experimental setup. Measured angle of rotation of linearly polarized light vs helix solid angle. Open circles represent the data for uniform helices; squares and triangle and solid circles represent nonuniform helices. The solid line is the theoretical prediction based on Berrys phase. From Ref. [20].

will be (omitting the dynamical phase)

$$|\chi'\rangle = \frac{\exp(i\gamma_+) |+\rangle + \exp(i\gamma_-) |-\rangle}{\sqrt{2}}, \quad (71)$$

with $\gamma_+ = -\gamma_- = -\Omega$, which yields

$$|\langle\chi'|\chi\rangle|^2 = \cos^2 \Omega. \quad (72)$$

By Malus' law, this means that the polarization has rotated by an angle Ω (the sense of rotation, when looking into the output of the fiber is counterclockwise, i.e., dextrorotatory, for a left-handed helix) [19].

The experiment carried out by Tomita and Chiao [20] is shown in Fig. 6, and shows a very good agreement between theoretical prediction and experimental results. Note that this kind of experiment can also be explained entirely from classical electrodynamics considerations [21].

6.3 Berry phase effects in nuclear magnetic resonance

Nuclear spins interact very weakly with each other and with their environment and therefore offer constitute systems that ideally suited to test the Berry phase of a single spin. The experi-

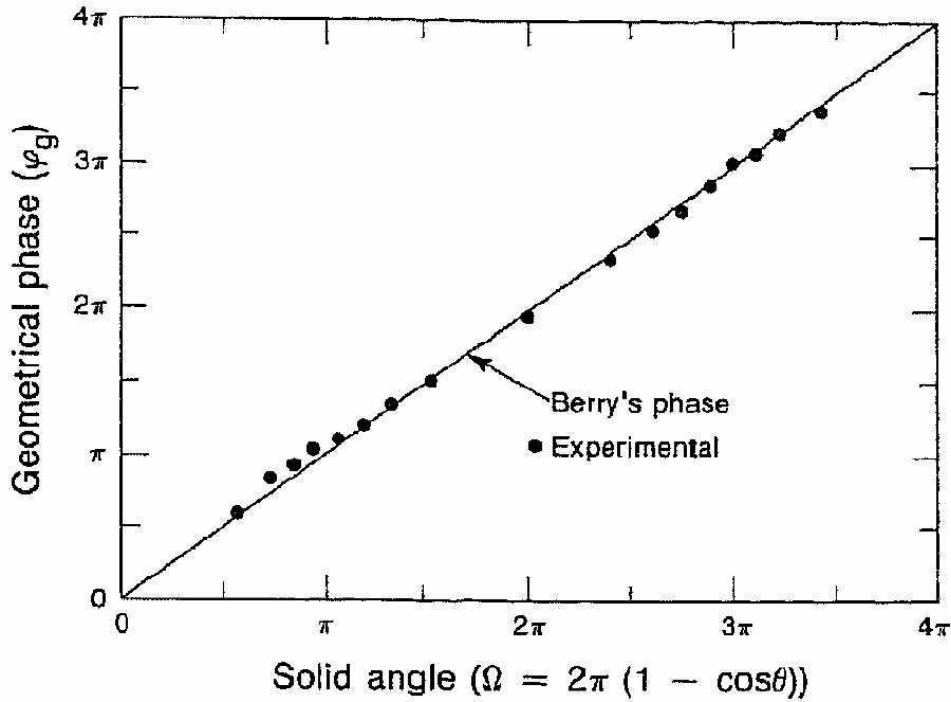


Fig. 7: NMR measurement of the Berry phase. From Ref. [22].

ment described below has been performed on protons ($S = 1/2$) by Suter *et al.* [22] following a proposal of Moody *et al.* [23].

As in a typical nuclear magnetic resonance (NMR) experiment, the spins are subject to a large, static, orienting field parallel to the z axis, and to a weak, transverse, field rotating around B_0 at angular frequency ω_{RF} . For convenience, we express here energies and magnetic fields in units of angular frequencies, i.e., the Hamiltonian, expressed in the laboratory frame, reads

$$H(t) = -\omega_L S_z - \omega_1 [S_x \cos(\omega_{\text{RF}} t) + S_y \sin(\omega_{\text{RF}} t)]. \quad (73)$$

The measured signal is the transverse magnetization $\langle S_x(t) + i \rangle, \langle S_y(t) \rangle$. In the present case, it is of convenient to perform a transformation from the laboratory frame to a detector frame, rotating at angular frequency ω_D . In practice, this is achieved by beating the measured signal against a reference signal of angular frequency ω_D . In the detector frame, the Hamiltonian now reads

$$H'(t) = -(\omega_L - \omega_D) S_z - \omega_1 [S_x \cos((\omega_{\text{RF}} - \omega_D)t) + S_y \sin((\omega_{\text{RF}} - \omega_D)t)]. \quad (74)$$

Let us define

$$\omega_{\text{eff}} \equiv \sqrt{(\omega_L - \omega_D)^2 + \omega_1^2}, \quad (75)$$

which is the magnitude of the total field in the detector frame, at angle $\theta \equiv \arcsin(\omega_1/\omega_{\text{eff}})$ from the z axis and precessing around the z axis at angular frequency $\omega_{\text{RF}} - \omega_D$. In the adiabatic limit, i.e., if $|\omega_{\text{RF}} - \omega_D| \ll \omega_{\text{eff}}$, the adiabatic eigenstates have an energy $\omega_n = -n\omega_{\text{eff}}$ ($n = \pm 1/2$). For each cycle of the effective field around the z axis, the state n acquires a Berry phase $\gamma_n = -n2\pi(1 - \cos\theta)$. Thus if we prepare the system in a superposition of the two

states $n = \pm 1/2$, the Fourier spectrum of the transverse magnetization will have a component of angular frequency $\omega_{\text{eff}} + (\omega_{\text{RF}} - \omega_D)2\pi(1 - \cos\theta)$, where the last term arising from the Berry phase, as shown in Fig. 7.

7 Berry phase for itinerant electrons in a solid

7.1 General formulation

We now want to discuss the Berry phase of electrons in solids. Let us consider (non-interacting) electrons subject to a scalar potential and to a Zeeman (or exchange) field, whose direction is spatially nonuniform. As they move through the solid, the electrons experience, in their proper reference frame, a Zeeman field whose direction changes with time. If this change is slow enough, the electron spin has to follow it adiabatically and therefore accumulates a Berry phase [24, 25, 26].

Before discussing the resulting physical consequences, let us formulate the problem more precisely. I follow here the discussion of Ref. [27]. The corresponding Hamiltonian is

$$H = -\frac{\hbar^2}{2m} \frac{\partial^2}{\partial \mathbf{r}^2} + V(\mathbf{r}) - \Delta(\mathbf{r}) \mathbf{n}(\mathbf{r}) \cdot \boldsymbol{\sigma}. \quad (76)$$

We use a gauge transformation $T(\mathbf{r})$, which makes the quantization axis oriented along vector $\mathbf{n}(\mathbf{r})$ at each point. It transforms the last term in the above equation as $T^\dagger(\mathbf{r}) [\boldsymbol{\sigma} \cdot \mathbf{n}(\mathbf{r})] T(\mathbf{r}) = \sigma_z$, corresponding to a local rotation of the quantization axis from z axis to the axis along $\mathbf{n}(\mathbf{r})$. The transformed Hamiltonian describes the electrons moving in a (spinor) gauge potential $\mathbf{A}(\mathbf{r})$,

$$H' \equiv T^\dagger H T = -\frac{\hbar^2}{2m} \left(\frac{\partial}{\partial \mathbf{r}} - \frac{ie}{\hbar c} \mathbf{A}(\mathbf{r}) \right)^2 + V(\mathbf{r}) - \Delta(\mathbf{r}) \sigma_z, \quad (77)$$

where $A_i(\mathbf{r}) = -2\pi i \phi_0 T^\dagger(\mathbf{r}) \partial_i T(\mathbf{r})$, $\phi_0 = hc/|e|$ is the flux quantum. For convenience, we have defined the gauge potential $\mathbf{A}(\mathbf{r})$ to have the same dimension as the electromagnetic vector potential. The components of $\mathbf{A}(\mathbf{r})$ can be found easily using an explicit form of $T(\mathbf{r})$.

The above Hamiltonian with the matrix $\mathbf{A}(\mathbf{r})$ contains terms coupling the two spin states. If the rate at which the spin-quantization axis varies is slow enough as compared to the Larmor precession frequency (as seen from the moving electron's frame), the spin will follow adiabatically the local spin-quantization axis, and these spin-flip terms can be neglected. The variation rate of the spin quantization axis is (for an electron at the Fermi level) v_F/ξ , where ξ is the characteristic length of variation of the spin-quantization axis, so that the adiabaticity condition is

$$\frac{\hbar v_F}{\xi} \ll \Delta. \quad (78)$$

With this approximation we now obtain

$$H' \simeq -\frac{\hbar^2}{2m} \left(\frac{\partial}{\partial \mathbf{r}} - \frac{ie}{\hbar c} \mathbf{a}(\mathbf{r}) \sigma_z \right)^2 + V(\mathbf{r}) + V'(\mathbf{r}) - \Delta(\mathbf{r}) \sigma_z, \quad (79)$$

where

$$a_i(\mathbf{r}) \equiv \frac{\pi \phi_0 (n_x \partial_i n_y - n_y \partial_i n_x)}{1 + n_z} \quad (80)$$

is an effective vector potential arising from the Berry phase, and

$$V'(\mathbf{r}) = (\hbar^2/8m) \sum_{i,\mu} (\partial_i n_\mu)^2 \quad (81)$$

is an effective scalar potential. Since the Hamiltonian is diagonal in spin, we can treat the two spin subbands separately. For each of the spin subband, we have mapped the original problem on the simpler one of a spinless electron moving in effective scalar and vector potentials. The effective vector potential in turn gives rise to an effective magnetic field $\mathbf{b} \equiv \nabla \times \mathbf{a}$, whose components are expressed in terms of the magnetization texture as

$$B_i = \frac{\phi_0}{4\pi} \varepsilon_{ijk} \varepsilon_{\mu\nu\lambda} n_\mu (\partial_j n_\nu) (\partial_k n_\lambda). \quad (82)$$

The physical consequences of the effective vector potential and effective magnetic field are exactly the same as those of the familiar electro-magnetic counterparts, and can be classified in two different classes:

1. local effects such as the Lorentz force. These effects are classical in origin (see the illuminating discussion on this point given by Aharonov and Stern [28]), and therefore do not require phase coherence.
2. non-local interference effects, such as Aharonov-Bohm-like effects and persistent currents. These effects are intrinsically quantum mechanical, and require phase coherence.

7.2 Anomalous Hall effect due to the Berry phase in a textured ferromagnet

The Hall effect consists in the appearance of a voltage transverse to the current in a conducting system. As it is antisymmetric with respect to time reversal, it may appear only in the presence of a term in the Hamiltonian breaking time reversal invariance. Until recently, two different mechanisms were recognized to give rise to the Hall effect:

1. the electro-magnetic Lorentz force due to a usual magnetic field; in the classical regime (normal Hall effect), this is well described by the Drude theory; in the quantum limit, the spectacular quantum Hall effect is obtained.
2. in absence of an external magnetic field, time-reversal invariance is also broken if the system exhibits magnetic order. However, this fact is not enough to induce a Hall effect if the magnetic order is uniform and spin-orbit coupling is absent or negligible, because the system is then invariant by under a global rotation of π of the spins, which is equivalent to time reversal in this case (uniform magnetization). Therefore Hall effect arises only as a consequence of simultaneous presence of spontaneous magnetic order and spin-orbit coupling. This mechanism is called the anomalous Hall effect.

Recently, however, it was realized that a third mechanism could give rise to the Hall effect in ferromagnetic, in absence of an external magnetic field, and of the spin-orbit coupling, if the

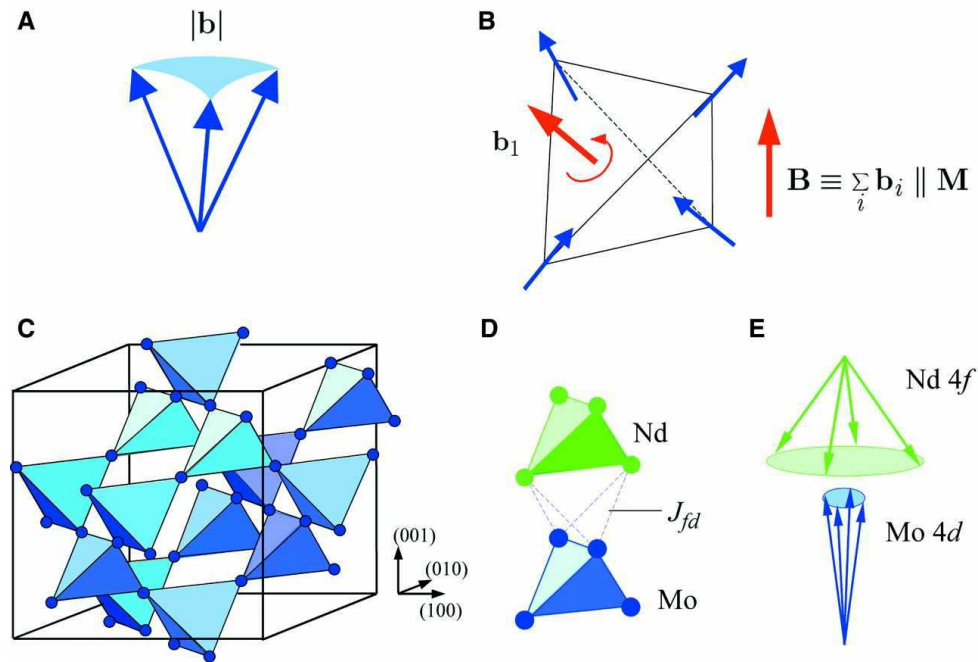


Fig. 8: Schematic magnetic and crystal structures of pyrochlore. (A) Spin chirality, that is, the solid angle subtended by the three spins. (B) “Two-in, two-out” spin structure, in which each spin points along the line that connects the center of the tetrahedron and the vertex. The total fictitious magnetic field is the vector sum of each fictitious magnetic flux that penetrates each plaquette. (C) The B sublattice of pyrochlore structure $A_2B_2O_7$. The A sublattice is structurally identical with this one, but is displaced by half a lattice constant. (D) Relative position of Nd tetrahedron (green circles) and Mo tetrahedron (blue circles) in $Nd_2Mo_2O_7$ pyrochlore. (E) The umbrella structure observed for $Nd_2Mo_2O_7$ ($A=Nd$, $B=Mo$) by a neutron diffraction study. From Ref. [33].

magnetization is non-uniform and exhibits a non-trivial texture [29, 30, 31, 32, 33, 34, 35, 36, 37, 38, 39, 40, 27].

The central idea is the following: as we have discussed above that if the spin-orbit coupling is negligible, the system is invariant under a global rotation of the magnetization. However, if the magnetization is non-uniform, a rotation of π is generally not equivalent to a time-reversal, so that Hall effect may arise. At the microscopic level, the origin of the Hall effect in such a case is the effective Lorentz force due to the Berry phase of the magnetization texture.

We shall discuss below as an example the results of Taguchi *et al.* [33]. In this work the authors investigated the compound $Nd_2Mo_2O_7$, which has the pyrochlore structure shown on Fig. 8. Due to their large spin-orbit coupling the Nd 4f moments of a given tetrahedron adopt the “two-in, two-out” structure shown on Fig. 8B. The Mo 4d moments which are ferromagnetically coupled to each other and antiferromagnetically to the the Nd moments therefore adopt and non-collinear umbrella structure, whose chirality gives rise to the anomalous Hall effect: as electrons moves on a triangle face of a tetrahedron, they acquire a Berry phase, and experience the associated Lorentz force. This mechanism is dominant at low temperature, where other mechanisms due to the spin-orbit coupling (giving contributions to the Hall resistivity

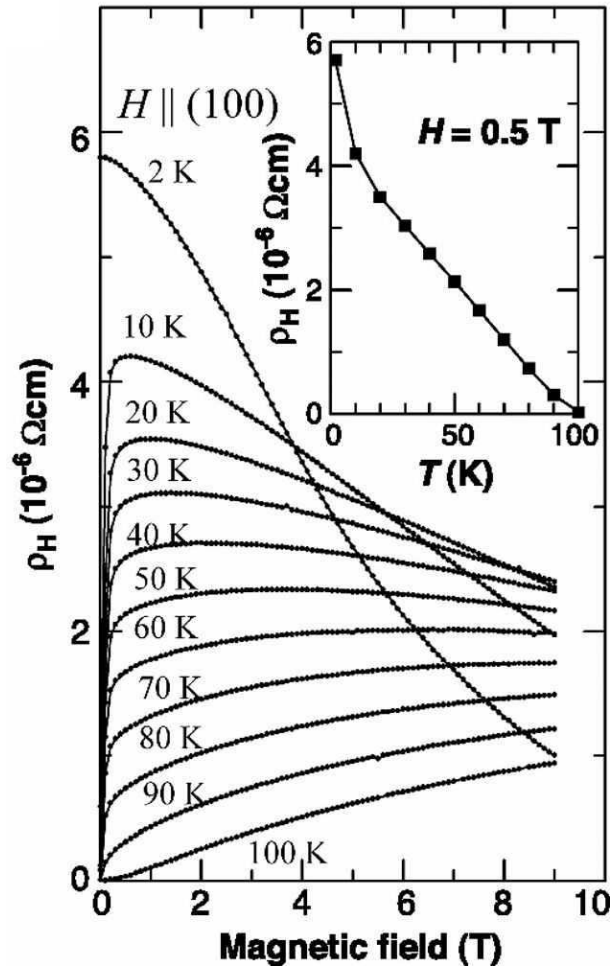


Fig. 9: Magnetic field dependence of the Hall resistivity ρ_H with $H \parallel (100)$ at several temperatures. The inset shows the temperature dependence of ρ_H at 0.5 T, which is a measure of the anomalous Hall term. The ρ_H at a low field ($< 0.3 \text{ T}$) is finite at 2 K, whereas it tends to zero above 10 K, in accord with the presence or absence of remnant magnetization at the respective temperatures. From Ref. [33].

linear or quadratic in the longitudinal resistivity) are strongly suppressed. That the origin of the anomalous Hall effect is the Berry phase due to the texture is further indicated by noting that the application of a magnetic field reduces the solid angle of the umbrella texture and hence the Berry phase and the associated Hall effect.

One should note, however, that the average effective magnetic field due to the Berry phase is zero on the present case. This can be understood by noting [31] that the Mo planes perpendicular to (111) axes are kagomé lattices, with a Berry phase of $+\varphi$ on the triangles and -2φ on the hexagons. Since there are two triangles and one hexagon per unit cell the effective magnetic field due to the Berry phase is zero on average. However, since the circuits with positive (triangles) and negative (hexagons) Berry phase are inequivalent, time reversal invariance is still broken, and a non zero Hall effect may (and generally does) result [31]. However, because the effective field due to the Berry phase vanishes on average, the resulting Hall effect is considerably weaker than that one would obtain for a non-zero net effective field.

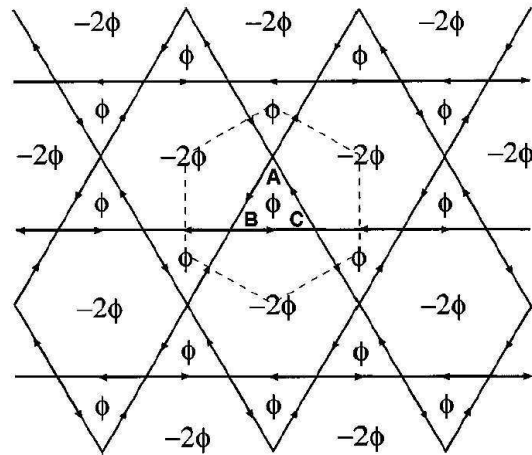


Fig. 10: Kagomé lattice. The dotted line represents the Wigner-Seitz unit cell, which contains three independent sites A, B, C . From Ref. [31].

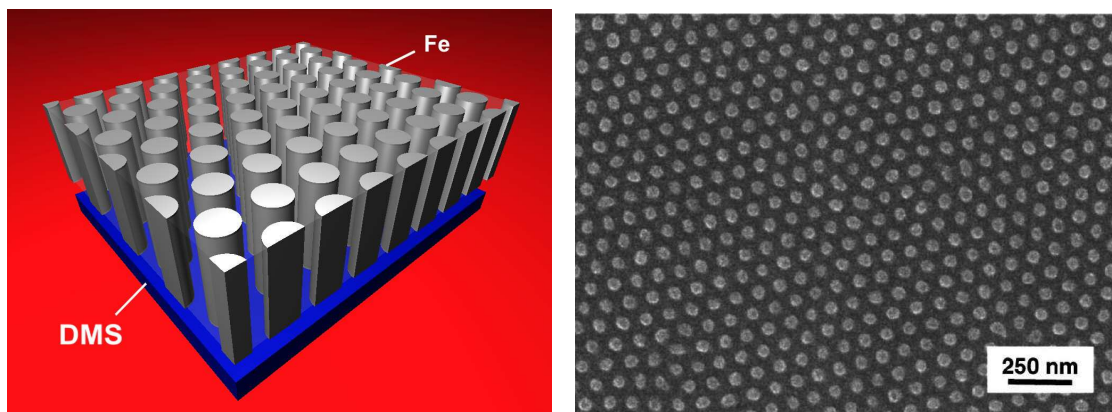


Fig. 11: Left: The proposed structure consisting of a triangular lattice of magnetic nanocylinders on top of 2D diluted magnetic semiconductor. From Ref. [27]. Right: Example of an triangular array of Ni nanocylinders (cylinder distance = 100 nm) in an alumina matrix. From Ref. [41].

One should also notice that, as in the example discussed above, spin-orbit coupling always has to be invoked in order to obtain a spin-texture with a definite chirality and, hence, a non-zero Hall effect [30, 32, 35, 38, 39]. This is, however, quite different from the mechanisms of Hall effect in which the spin-orbit coupling directly influences the motion of the conduction electrons.

Until recently, all cases of anomalous Hall due to a chiral spin texture discussed in the literature considered a texture at the atomic level. Recently, it has been proposed that a mesoscopic scale magnetic field texture can be produced by using magnetic nanostructures [27]. For example, one can consider an array of magnetic nanocylinders (all magnetized in the same direction along their axis), as shown in Fig. 11 (left panel), in order to generate a non-uniform dipolar stray field in a two-dimensional electron (or hole) gas placed just underneath. Such structure can be fabricated by electrolytic techniques, as shown on Fig. 11 (right panel).

The Fig. 12 shows the z -component of the dipolar stray field (left panel) and topological field generated by the Berry phase (right). It is noteworthy that for a lattice of Fe cylinders with a pitch of 100 nm, the dipolar field at a distance 20 nm underneath (the average value of which is always zero) has a maximum absolute value of about 2 kG, whereas the topological field has a non-zero average value of about 5 kG, with local values ranging between -5 and $+15$ kG. Thus, one sees that a rather weak dipolar stray field averaging to zero generates in the two-dimensional electron gas a much stronger topological field with a non-zero average!

The topological field has a number of interesting properties:

- First, one can show that the total flux of the topological field through a unit cell is always an integer multiple of the flux quantum. To see this, let us consider the Berry phase corresponding to circuit going around a unit cell (e.g., along the path ABCDA on Fig. 13 (left panel). Because of the translational periodicity of the system, the local field points along the same direction at the four corners A, B, C, D of the unit cell, and thus correspond to the same point (represented by the solid dot) on the sphere of unit radius on which the corresponding path for the field direction takes place; the path ABC is shown, and one sees immediately that, because of the translational periodicity, the path CDA is exactly the same, described in the reversed direction, so that the Berry phase corresponding to the path ABCDA is zero modulo 2π which implies the quantization of the total flux in units of ϕ_0 . This constitutes an example of topological quantization.
- Next, let us try to understand what is the actual integer value taken by the total topological flux. The above reasoning does tell us anything about it, because we don't know how many times we are wrapping the sphere when integrating over the unit cell. To know this, we may consider the closed lines where the z -component of the stray field vanishes. This lines corresponds to paths going an integer number of times around the “equator” of the unit sphere. Such lines are shown on Fig. 12 (left panel, solid lines). One can then see that each round trip around the equator contributes to one flux quantum. In counting this, one should be careful in getting the sign correctly. In the case shown in Fig. 12 for a vanishing external field, one obtains that the total topological flux per unit cell is $+\phi_0$.
- Finally, one can see that the lines of zero z -component of the stray field will change if one applies an external magnetic field. For example, in the case considered here, under application of a uniform external field along the magnetization direction of the nanocylin-

ders, the regions of positive z -field will expand, so that the topology of the lines of zero z -field will eventually change. This is shown by the dashed lines on the left panel of Fig.12 ($B_{\text{ext}}/4\pi M_s = 0.058$). From the above discussion, this implies a change in the topological flux per unit cell, which now takes the value $-2\phi_0$ (the factor 2 is because there are 2 lines per unit cell, and the factor -1 is because the circulation is reversed).

The properties discussed above indicate that by application an a rather small uniform external field, one can change the average value of the topological field. This will give rise to changes in the anomalous Hall effect. As a first approximation, one can estimate the Hall effect by using the Drude model and by neglecting the spacial fluctuations of the dipolar and topological fields. In this case, the Hall effect is just given by the familiar Drude formula, with an effective field equal to the sum of the external magnetic field and the average topological field. If the two spin subbands contribute, one simply has to sum the contributions of the two subbands, taking into account the fact that the topological field is of opposite sign for the two spin subbands. For the case discussed here, and assuming that only one spin subband is occupied, the resulting behavior of the Hall effect is shown on Fig. 14. For the chosen parameters, the values of the critical fields are $B_1 \simeq -2$ kG, $B_2 \simeq 0.9$ kG, and $B_3 \simeq 1.3$ kG. The uniform slope comes from the normal Hall effect (Lorentz force of the external magnetic field), whereas the remaining non-monotonous contribution arises from the Lorentz force due to the topological field of the Berry phase. Such a characteristic non-monotonous behavior would constitute a signature of the Berry phase contribution of the Hall effect and can be tested experimentally. One should point out, however, that in the vicinity of the critical fields where the topological flux abruptly changes, the adiabaticity condition cannot be well satisfied, so that, in practice, a rounded curve would be obtained.

In order to identify a system for which the above predictions can be satisfied, we have to look for a system with a large Zeeman splitting, in order to satisfy as well as possible the condition of adiabaticity. We propose to use II-VI dilute magnetic semiconductors (DMS) which exhibit giant Zeeman splitting; p-type Mn doped DMS are best suited since the exchange constants for holes are much larger than for electrons [42, 43]. For a detailed discussion see Ref. [27].

Before closing this section on the anomalous Hall effect, I wish to point that, while the Berry phase allowed to identified a new mechanism of Hall effect arising from the chirality of the spin texture, in absence of an external field and of the spin-orbit coupling, as we have discussed above, it also allows to give a modern interpretation to the previously known mechanisms for the Hall effect (normal Hall effect, classical or quantized; anomalous Hall effect), due either to an external magnetic field, or to the spin-orbit coupling. In this case, one deals with Berry phase in momentum space instead of real space as discussed above. For a detailed discussion, see Refs. [44, 45, 46, 47, 48, 49, 50, 51, 52, 53, 54, 55, 56].

7.3 Interference effects due to the Berry phase in an Aharonov-Bohm ring

As mentioned earlier, the Berry phase accumulated by electrons moving in a non-trivial magnetic texture can give rise to interference effects, of which the archetype is the Aharonov-Bohm effect. It has been proposed by Loss *et al.* [24, 26] and by Stern [25] that a metallic ring subject to a textured magnetic field (or magnetization) as depicted in Fig. 15 would yield a Berry phase for an electron moving around the ring, and hence a dependence of the conductance of the ring

(when connected to current leads) upon the solid angle described by the magnetization [25, 57], as well as to persistent charge and spin currents (for a non-connected ring) [24, 26].

So far, it has not been possible to test experimentally this prediction in the configuration described above (i.e., by using a textured magnetic field or magnetization). However, several authors [58, 59] have indicated that a similar Berry phase may be obtained by using the combined effect of the Zeeman coupling to a uniform magnetic field (parallel to the ring axis) and of Rashba-type spin-orbit coupling [60, 61], as described by the following Hamiltonian

$$H = \frac{\mathbf{p}^2}{2m} - B\sigma_z + \alpha(\mathbf{p} \times \boldsymbol{\sigma}) \cdot \hat{\mathbf{z}} + V(\mathbf{r}). \quad (83)$$

In the above equation, the third term gives the Rashba spin-orbit coupling, while the last one confines the electron to the ring. The Rashba effect acts as an effective magnetic field perpendicular to the plane and to the direction of motion.

There is, however, a crucial difference with respect to a true magnetic field, namely that the Rashba term is invariant under time reversal (unlike a true magnetic field), which is manifest from the fact the associated effective field changes sign as the motion is reversed. Because of this, there is no phase shift from the Berry phase between the paths going through the upper and lower arms of the ring, as sketched on Fig. 16, unlike what would be expected for a real magnetic field as in Fig. 15. Therefore, Aharonov-Bohm like interferences in this configuration have to involve paths that wind completely the ring a different number of times. The associated Berry phase will of course be superimposed to the usual Aharonov-Bohm phase and therefore modify the Aharonov-Bohm oscillations of the ring conductance versus magnetic field. Such observations, indicating the presence of the Berry phase, have been made by various groups [62, 63, 64]. The results of Mopurgo *et al.* [62] are shown in Fig. 17, where the signature of the Berry phase is given by the splitting of the e/h peak in the average Fourier spectrum.

8 Further effects of Berry phase in magnetism

In closing these lecture notes, I wish to briefly mention some further developments and applications of the concept of Berry phase in magnetism.

In the previous section, we mentioned that the Berry phase can give rise to interference phenomena for interfering paths in real space. There may be also interferences associated with different paths in spin space as well; this plays an important role in the theory of tunnelling of magnetization in large spin molecular magnets [65, 66, 67]. The situation is sketched in Fig. 18. Depending on the value of the spin, and on the solid angle between the 2 tunnelling trajectories from state A to state B, interference due to the Berry phase take place; in special cases, the interferences are destructive and tunnelling becomes forbidden. This gives rise to very spectacular parity effect that have been observed experimentally [69, 70, 71]. For a detailed review of this topic, see Ref. [72].

The Berry phase plays a ubiquitous role in quantum mechanical problems where one wants to treat the dynamics of some “slow” degrees of freedom, after having “integrated out” the “fast” degrees of freedom. An application of this concept in magnetism concerns the adiabatic spin-wave dynamics of itinerant magnets. Here the fast degrees of freedom are the electron degrees

of freedom giving rise to charge fluctuations and longitudinal spin fluctuations, whereas the slow degrees of freedom are the transverse spin fluctuations, i.e., the long wavelength magnons. This was pioneered by Wen and Zee [73], and later on further developed by Niu *et al.* [74, 75]. They obtained an equation of motion for the spins which is controlled by the Berry phase; in the case of localized systems, this reduces to the Landau-Lifshitz equation, but contains non-local contributions in the case of strongly delocalized systems.

For a spin S coupled to a slowly moving magnetic field, we have seen that the Berry phase is given by the solid angle described by the field. For the case of a spin $S = 1/2$, this situation constitutes the most general case, however, for larger spins $S \geq 1$, the most general Hamiltonian may contain more further contributions, such as anisotropy terms, so that the parameter space is much larger and richer than for a spin $1/2$. It is therefore of interest to investigate the Berry phase in this more general context. Recently, this has been investigated, by considering more specifically the Berry phase associated with global rotations of anisotropic spin systems [76]. This study reveals that beside the familiar solid angle term, there is also a topological term, related to a winding number giving the number of rotations of the systems around its magnetization axis. This is relevant to any spin system of spin $S \geq 1$, in particular to magnons ($S = 1$), holes in semiconductors ($S = 3/2$), etc. A general theory of the Berry phase of magnons is in preparation [77]. Interesting spin-wave interference phenomena have recently been obtained by Hertel *et al.* from micromagnetic simulations [78].

References

- [1] M.V. Berry, Proc. Roy. Soc. London A **392**, 45 (1984).
- [2] *Geometric Phases in Physics*, edited by A. Shapere and F. Wilczek (World Scientific, Singapore, 1989).
- [3] A. Bohm, A. Mostafazadeh, H. Koizumi, Q. Niu, and J. Zwanziger, *The Geometric Phase in Quantum Systems* (Springer Verlag, Berlin, 2003).
- [4] M.V. Berry, in *Anomalies, phase, defects*, p. 125, edited by U.M. Bregola, G. Marmo, and G. Morandi (Bibliopolis, Naples, 1990); also available at <http://www.phy.bris.ac.uk/research/theory/Berry>.
- [5] J.H. Hannay, J. Phys. A: Math. Gen. **18**, 221 (1985).
- [6] M.V. Berry, J. Phys. A: Math. Gen. **18**, 15 (1985).
- [7] A. Messiah, *Quantum Mechanics*, Vol. 2 (North Holland, Amsterdam, 1991).
- [8] S. Pancharatnam, Proceedings of the Indian Academy in Sciences, **44**, 247 (1956); also reprinted in Ref. [2].
- [9] Y. Aharonov and D. Bohm, Phys. Rev. **115**, 485 (1959).
- [10] C.A. Mead and D.G. Truhlar, J. Chem. Phys. **70**, 2284 (1989).
- [11] J. von Neumann and E.P. Wigner, Phys. Z. **30**, 467 (1929).
- [12] P.A.M. Dirac, Proc. Roy. Soc. London A **133**, 60 (1931); Phys. Rev. **74**, 817 (1948).
- [13] A. Tonomura, N. Osakabe, T. Matsuda, T. Kawasaki, J. Endo, S. Yano, and H. Yamada, Phys. Rev. Lett. **56**, 792 (1986).
- [14] S. Olariu and I.I. Popescu, Rev. Mod. Phys. **57**, 339 (1985).
- [15] A.G. Aronov and Y.V. Sharvin, Rev. Mod. Phys. **59**, 755 (1987).
- [16] S. Washburn and R.A. Webb, Rep. Prog. Phys. **55**, 1311 (1992).
- [17] J.A. Cina, Chem. Phys. Lett. **132**, 393 (1986).
- [18] T. Bitter and D. Dubbers, Phys. Rev. Lett. **59**, 251 (1987).
- [19] R.Y. Chiao and Y.S. Wu, Phys. Rev. Lett. **57**, 933 (1986).
- [20] A. Tomita and R.Y. Chiao, Phys. Rev. Lett. **57**, 937 (1986).
- [21] M.V. Berry, Nature **326**, 277 (1987).
- [22] D. Suter, G.C. Chingas, R.A. Harris, and A. Pines, Molec. Phys. **61**, 1327 (1987).
- [23] J. Moody, A. Shapere, and F. Wilczek, Phys. Rev. Lett. **56**, 893 (1986).

- [24] D. Loss, P. Goldbart, and A.V. Balatsky, *Phys. Rev. Lett.* **65**, 1655 (1990).
- [25] A. Stern, *Phys. Rev. Lett.* **68**, 1022 (1992).
- [26] D. Loss, and P.M. Goldbart, *Phys. Rev. B* **45**, 13544 (1992).
- [27] P. Bruno, V.K. Dugaev, and M. Taillefumier, *Phys. Rev. Lett.* **93**, 096806 (2004).
- [28] Y. Aharonov and A. Stern, *Phys. Rev. Lett.* **69**, 3593 (1992).
- [29] P. Matl, N.P. Ong, Y.F. Yan, Y.Q. Li, D. Studebaker, T. Baum, and G. Doubinina, *Phys. Rev. B* **57**, 10248 (1998).
- [30] J. Ye, Y.B. Kim, A.J. Millis, B.I. Shraiman, P. Majumdar, and Z. Tešanović, *Phys. Rev. Lett.* **83**, 3737 (1999).
- [31] K. Ohgushi, S. Murakami, and N. Nagaosa, *Phys. Rev. B* **62**, 6065 (2000).
- [32] S.H. Chun, M.B. Salamon, Y. Lyanda-Geller, P.M. Goldbart, and P.D. Han, *Phys. Rev. Lett.* **84**, 757 (2000).
- [33] Y. Taguchi, Y. Oohara, H. Yoshizawa, N. Nagaosa, and Y. Tokura, *Science* **291**, 2573 (2001).
- [34] Y. Taguchi and Y. Tokura, *Europhys. Lett.* **54**, 401 (2001).
- [35] Y. Lyanda-Geller, S.H. Chun, M.B. Salamon, P.M. Goldbart, P.D. Han, Y. Tomioka, A. Asamitsu, and Y. Tokura, *Phys. Rev. B* **63**, 184426 (2001).
- [36] N. Nagaosa, *Mat. Sci. Eng. B* **84**, 58 (2001).
- [37] H. Yanagihara and M.B. Salamon, *Phys. Rev. Lett.* **89**, 187201 (2002).
- [38] G. Tatara and H. Kawamura, *J. Phys. Soc. Japan* **71**, 2613 (2002).
- [39] S. Onoda and N. Nagaosa, *Phys. Rev. Lett.* **90**, 196602 (2003).
- [40] Y. Taguchi, T. Sasaki, S. Awaji, Y. Iwasa, T. Tayama, T. Sakakibara, S. Iguchi, T. Ito, and Y. Tokura, *Phys. Rev. Lett.* **90**, 257202 (2003).
- [41] K. Nielsch, R.B. Wehrspohn, J. Barthel, J. Kirschner, U. Gösele, S.F. Fischer and H. Kronmüller, *Appl. Phys. Lett.* **79**, 1360 (2001).
- [42] J.K. Furdyna, *J. Appl. Phys.* **64**, R29 (1988).
- [43] J. Kossut and W. Dobrowolski, in *Handbook of Magnetic Materials*, edited by K. H. J. Buschow (Elsevier, Holland, 1993), Vol. **7**, p. 231.
- [44] B. Simon, *Phys. Rev. Lett.* **51**, 2167 (1983).
- [45] M. Kohmoto, *Ann. Phys. (New York)* **160**, 343 (1985).
- [46] Q. Niu, D.J. Thouless, and Y.S. Wu, *Phys. Rev. B* **31**, 3372 (1985).

- [47] M. Kohmoto, J. Phys. Soc. Japan **62**, 659 (1993).
- [48] M.C. Chang and Q. Niu, Phys. Rev. B **53**, 7010 (1996).
- [49] G. Sundaram and Q. Niu, Phys. Rev. B **59**, 14915 (1999).
- [50] T. Jungwirth, Q. Niu, and A.H. MacDonald, Phys. Rev. Lett. **88**, 207208 (2002).
- [51] M. Onoda and N. Nagaosa, J. Phys. Soc. Japan **71**, 19 (2002).
- [52] S. Onoda and N. Nagaosa, Phys. Rev. Lett. **90**, 206601 (2003).
- [53] Z. Fang, N. Nagaosa, K.S. Takahashi, A. Asamitsu, R. Mathieu, T. Ogasawara, H. Yamada, M. Kawasaki, Y. Tokura, and K. Terakura, Science **302**, 92 (2003).
- [54] D. Culcer, A.H. MacDonald, and Q. Niu, Phys. Rev. B **68**, 045327 (2003).
- [55] Y. Yao, L. Kleinman, A.H. MacDonald, J. Sinova, T. Jungwirth, D.S. Wang, E. Wang, and Q. Niu, Phys. Rev. Lett. **92**, 037204 (2004).
- [56] F.D.M. Haldane, Phys. Rev. Lett. **93**, 206602 (2004).
- [57] A. Stern, in *Mesoscopic Electron Transport*, ed. by L.L. Sohn *et al.* (Kluwer, 1997), p. 45.
- [58] A.G. Aronov and Y.B. Lyanda-Geller, Phys. Rev. Lett. **70**, 343 (1993).
- [59] T.Z. Qian and Z.B. Su, Phys. Rev. Lett. **72**, 2311 (1994).
- [60] E.I. Rashba, Soviet Phys. Solid State **2**, 1109 (1960).
- [61] Y.A. Bychkov and E.I. Rashba, J. Phys. C **17**, 6039 (1984).
- [62] A.F. Morpurgo, J.P. Heida, T.M. Klapwijk, B.J. van Wees, and G. Borghs, Phys. Rev. Lett. **80**, 1050 (1998).
- [63] J.B. Yau, E.P. De Poortere, and M. Shayegan, Phys. Rev. Lett. **88**, 146801 (2002).
- [64] M.J. Yang, C.H. Yang, Y.B. Lyanda-Geller, Europhys. Lett. **66**, 826 (2004).
- [65] D. Loss, D.P. DiVincenzo, and G. Grinstein, Phys. Rev. Lett. **69**, 3232 (1992).
- [66] J. van Delft and C.L. Henley, Phys. Rev. Lett. **69**, 3236 (1992).
- [67] A. Garg, Europhys. Lett. **22**, 205 (1993).
- [68] D. Loss, in *Dynamical Properties of Unconventional Magnetic Systems*, ed. by A.T. Skjeltorp and D. Shewington (Kluwer, 1998), p. 29.
- [69] W. Wernsdorfer and R. Sessoli, Science **284**, 133 (1999).
- [70] W. Wernsdorfer, M. Soler, G. Christou, and D.N. Hendrickson, J. Appl. Phys. **91**, 7164 (2002).
- [71] E. del Barco, A.D. Kent, E.M. Rumberger, D.N. Hendrickson, and G. Christou, Phys. Rev. Lett. **91**, 047203 (2003).

-
- [72] D. Gatteschi and R. Sessoli, *Angew. Chem. Int. Edit.* **42**, 268 (2003).
- [73] X.G. Wen and A. Zee, *Phys. Rev. Lett.* **61**, 1025 (1988).
- [74] Q. Niu and L. Kleinman, *Phys. Rev. Lett.* **80**, 2205 (1998).
- [75] Q. Niu, X. Wang, L. Kleinman, W.M. Liu, D.M.C. Nicholson, and G.M. Stocks, *Phys. Rev. Lett.* **83**, 207 (1999).
- [76] P. Bruno, *Phys. Rev. Lett.* **93**, 247202 (2004).
- [77] V.K. Dugaev, P. Bruno, B. Canals, and C. Lacroix, *Phys. Rev. B* (in press); cond-mat/0503013.
- [78] R. Hertel, W. Wulfhekel, and J. Kirschner, *Phys. Rev. Lett.* **93**, 257202 (2004).

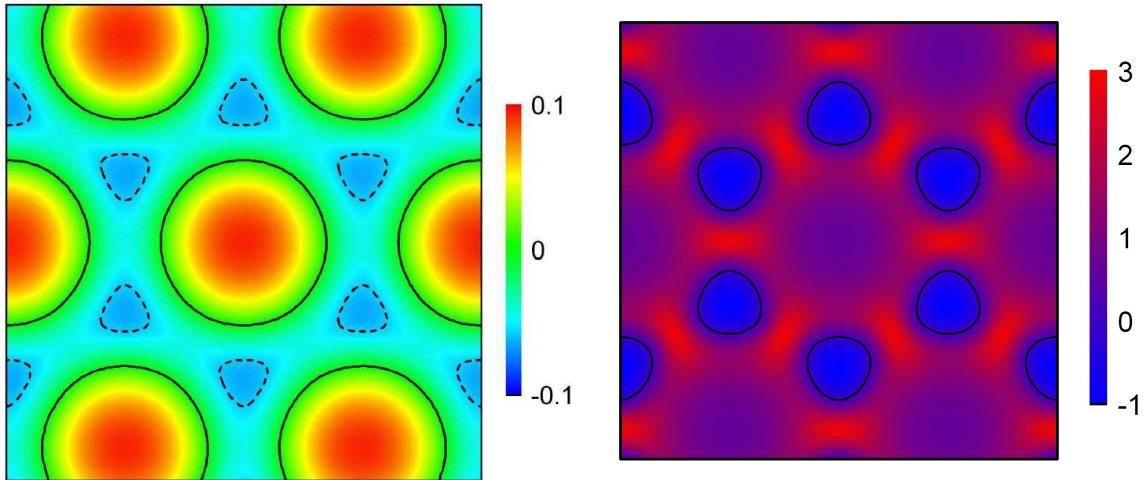


Fig. 12: *Left: Distribution of the z -component of dipolar field $B/4\pi M_s$ inside the semiconductor film for the triangular lattice of magnetic nanocylinders, for a zero external field. The black solid circles correspond to the lines with $B_z = 0$. Dashed lines correspond to the lines with $B_z = 0$ under a uniform external magnetic field $B_{\text{ext}}/4\pi M_s = 0.058$. Right: Topological field $B_t(\mathbf{r})$ (in units of ϕ_0 per unit cell area) for the triangular lattice of magnetic nanocylinders. From Ref. [27].*

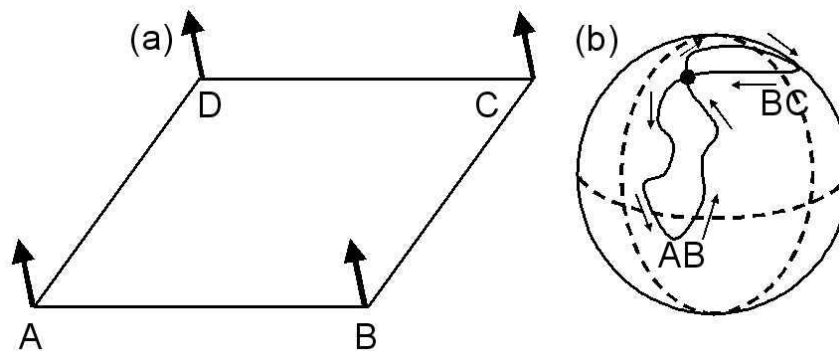


Fig. 13: *(a) unit cell in real space; (b) paths AB and BC on the sphere of unit radius.*

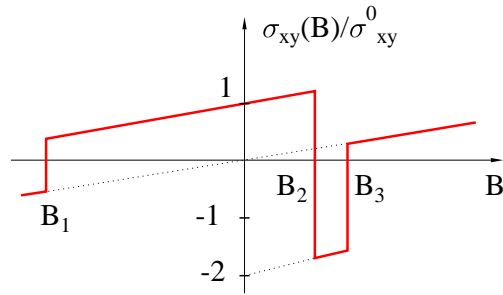


Fig. 14: Dependence of the Hall conductivity on external magnetic field (schematically). The slope corresponds to the contribution of the normal Hall effect; σ_{xy}^0 is the Hall conductivity corresponding to a topological flux per unit cell equal to ϕ_0 . From Ref. [27].

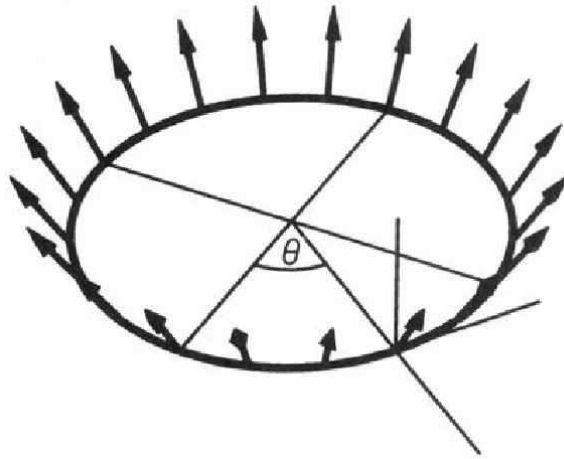


Fig. 15: Texture of the magnetic field (or magnetization) in a metallic ring. From Ref. [26].

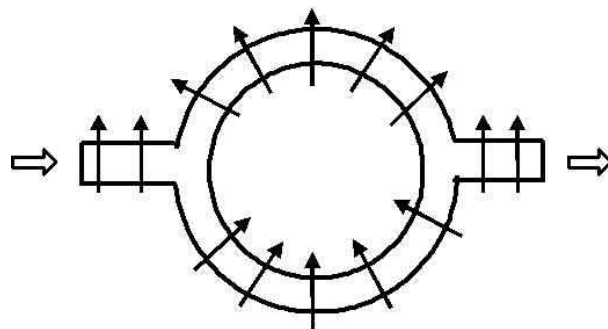


Fig. 16: Sketch of the effective field due to the Rashba effect for an electron moving from the left lead to the right lead.

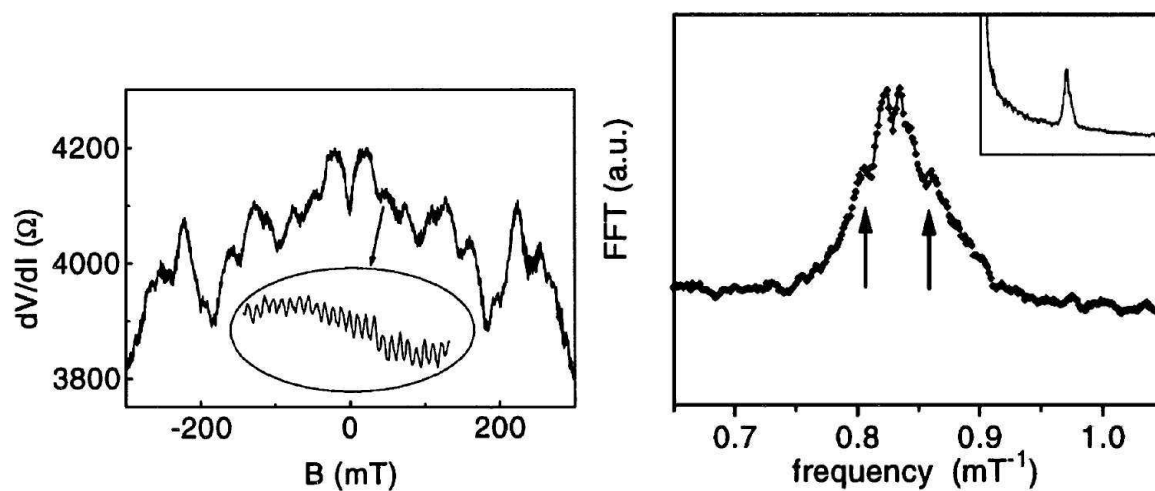


Fig. 17: Left panel: average of about 30 curves $R(B)$ (the inset is an enlargement of the small part of the curve). Right panel: the peak of the average Fourier spectrum: the splitting is evident, as well as some structure on the sides (pointed by the arrows). The inset shows the same curve on a larger frequency range. From Ref. [62]

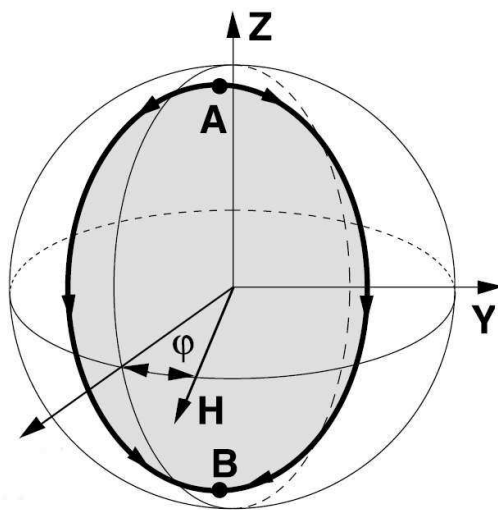


Fig. 18: Sketch of the Berry phase involved in the interference between 2 tunnelling paths between the spin states A and B. From Ref. [69]